Applied Radiation and Isotopes 215 (2025) 111562

Contents lists available at ScienceDirect

Applied Radiation and Isotopes

journal homepage: www.elsevier.com/locate/apradiso

^{111}Ag phantom images with Cerenkov Luminescence Imaging and digital autoradiography within the ISOLPHARM project

Davide Serafini [a,b,*,1], Nicola Zancopè [c,1], Anna Maria Pavone [d,e,1], Viviana Benfante [e,f], Alberto Arzenton [a,b], Vincenzo Russo [d], Michele Ballan [a], Luca Morselli [a,g], Francesco Paolo Cammarata [f,h], Albert Comelli [e], Giorgio Russo [f,h], Fabrizio Scopelliti [i], Valerio Di Marco [j], Francesca Mastrotto [k], Mattia Asti [l], Devid Maniglio [m], Carla Sbarra [n], Silva Bortolussi [o], Antonietta Donzella [p,q], Aldo Zenoni [p,q], Andrea Gandini [r], Valerio Villa [p,q], Diego Paderno [p,q], Lisa Zangrando [s], Stefano Corradetti [a], Emilio Mariotti [b,t], Andrea Salvini [r], Filippo Torrisi [u], Marcello Lunardon [c,s], Alberto Andrighetto [a]

[a] *Legnaro National Laboratories, National Institute for Nuclear Physics, INFN-LNL, Viale dell'Università 2, 35020 Legnaro, Italy*
[b] *Department of Physical Sciences, Earth and Environment, University of Siena, Via Roma 56, 53100 Siena, Italy*
[c] *Department of Physics and Astronomy, University of Padova, Via Marzolo 8, 35131 Padova, Italy*
[d] *Department of Biomedical and Biotechnological Sciences, University of Catania, Via Santa Sofia 97, 95123 Catania, Italy*
[e] *Ri.MED Foundation, Via Bandiera 11, 90133 Palermo, Italy*
[f] *Institute of Molecular Bioimaging and Physiology, National Research Council. IBFM-CNR, Contrada Pietrapollastra-Pisciotto, 90015 Cefalù, Italy*
[g] *Department of Physics and Earth Science, University of Ferrara, Via G. Saragat 1, 44121 Ferrara, Italy*
[h] *Laboratori Nazionali del Sud, National Institute for Nuclear Physics, INFN-LNS, Via Santa Sofia 62, 95123 Catania, Italy*
[i] *Nuclear Medicine Department of Cannizzaro Hospital, Via Messina 829, 95126 Catania, Italy*
[j] *Department of Chemical Sciences, University of Padova, Via Marzolo 1, 35131 Padova, Italy*
[k] *Department of Pharmaceutical and Pharmacological Sciences, University of Padova, Via Marzolo 5, 35131 Padova, Italy*
[l] *Radiopharmaceutical Chemistry Section, Nuclear Medicine Unit, AUSL-IRCCS di Reggio Emilia, Viale Risorgimento 80, 42122 Reggio Emilia, Italy*
[m] *Department of Industrial Engineering, BIOtech Research Center, University of Trento, Via delle Regole 101, 38123 Mattarello, Italy*
[n] *Bologna Division, National Institute for Nuclear Physics, Viale C. Berti Pichat 6/2, 40127 Bologna, Italy*
[o] *Department of Physics, University of Pavia, Via Bassi 6, 27100 Pavia, Italy*
[p] *Department of Mechanical and Industrial Engineering, University of Brescia, Via Branze 38, 25123 Brescia, Italy*
[q] *Pavia Division, National Institute for Nuclear Physics, Via Bassi 6, 27100 Pavia, Italy*
[r] *Applied Nuclear Energy Laboratory, LENA, Via G. Aselli 41, 27100 Pavia, Italy*
[s] *Padova Division, National Institute for Nuclear Physics, Via Marzolo 8, 35131 Padova, Italy*
[t] *Pisa Division, National Institute for Nuclear Physics, Largo Bruno Pontecorvo 3, 56127 Pisa, Italy*
[u] *Department of Medicine and Surgery, University of Enna "Kore", Via Marzolo 8, 35131 Enna, Italy*

ARTICLE INFO

Keywords:
^{111}Ag
^{68}Ga
Targeted radionuclide therapy

ABSTRACT

Targeted Radionuclide Therapy (TRT) is a medical technique exploiting radionuclides to combat cancer growth and spread. TRT requires a supply of radionuclides that are currently produced by either cyclotrons or nuclear research reactors. In this context, the ISOLPHARM project investigates the production of innovative radionuclides for medical applications. This production will be based on the forthcoming SPES facility at the

* Corresponding author at: Department of Physical Sciences, Earth and Environment, University of Siena, Via Roma 56, 53100 Siena, Italy.
E-mail addresses: davide.serafini@lnl.infn.it (D. Serafini), nicola.zancope@studenti.unipd.it (N. Zancopè), am.pavone8@gmail.com (A.M. Pavone), vbenfante@fondazionerimed.com (V. Benfante), alberto.arzenton@lnl.infn.it (A. Arzenton), r.vincenzosimone@gmail.com (V. Russo), michele.ballan@lnl.infn.it (M. Ballan), luca.morselli@lnl.infn.it (L. Morselli), francesco.cammarata@ibfm.cnr.it (F.P. Cammarata), acomelli@fondazionerimed.com (A. Comelli), giorgio-russo@cnr.it (G. Russo), Fabrizio.scopelliti@gmail.com (F. Scopelliti), valerio.dimarco@unipd.it (V.D. Marco), francesca.mastrotto@unipd.it (F. Mastrotto), Mattia.Asti@ausl.re.it (M. Asti), devid.maniglio@unitn.it (D. Maniglio), carla.sbarra@bo.infn.it (C. Sbarra), silva.bortolussi@unipv.it (S. Bortolussi), antonietta.donzella@unibs.it (A. Donzella), aldo.zenoni@unibs.it (A. Zenoni), andrea.gandini@unipv.it (A. Gandini), valerio.villa@unibs.it (V. Villa), diego.paderno@unibs.it (D. Paderno), lisa.zangrando@pd.infn.it (L. Zangrando), stefano.corradetti@lnl.infn.it (S. Corradetti), emilio.mariotti@unisi.it (E. Mariotti), andrea.salvini@unipv.it (A. Salvini), filippo.torrisi@unikore.it (F. Torrisi), marcello.lunardon@pd.infn.it (M. Lunardon), alberto.andrighetto@lnl.infn.it (A. Andrighetto).
[1] These authors contribute equally to the paper.

https://doi.org/10.1016/j.apradiso.2024.111562
Received 15 March 2024; Received in revised form 8 October 2024; Accepted 21 October 2024
Available online 28 October 2024

ISOLPHARM
Cerenkov luminescence imaging
Autoradiography
Radiopharmaceuticals

Legnaro National Laboratories (LNL) of the National Institute for Nuclear Physics (INFN), an ISOL facility where high-purity radioactive beams will be used to produce carrier-free radiopharmaceuticals. Previous studies demonstrated that a significant amount of ^{111}Ag, an innovative β/γ emitter suitable for TRT with theranostic applications, can be obtained at the SPES facility. The present work describes the first imaging study on phantoms with ^{111}Ag performed by the ISOLPHARM collaboration. This is a fundamental step to pave the way for the upcoming *in vivo* studies on the ^{111}Ag-based radiopharmaceutical currently being developed. The imaging potential of this radionuclide was investigated by acquiring phantom images with Cerenkov Luminescence Imaging (CLI) and digital autoradiography (ARG).

1. Introduction

In the last few years, Targeted Radionuclide Therapy (TRT) has shown notable potential as a strategy in cancer treatments (Brosch-Lenz et al., 2023). This approach relies on guiding radioactive isotopes toward tumor-associated targets, where accumulation occurs. At this site, a significant amount of ionizing radiation is released, with emission depending on the selected radioisotope (α, β and γ) (Morris et al., 2021). Focusing the biological effect of ionizing radiation solely on the target disease site enables the preservation of surrounding healthy tissues. Diagnostics and treatments can both be performed using this emission (theranostics). Indeed, radiopharmaceuticals' accumulation may be visualized by nuclear medicine imaging techniques, such as Positron Emission Tomography (PET) or Single Photon Emission Computed Tomography (SPECT), to evaluate the efficacy of the targeting agent for therapeutic approaches (Xue et al., 2021; Sun et al., 2023; Rowland and Cherry, 2008).

In recent years, advances in radiopharmaceutical development, vector technology, and labeling efficiency have contributed to the improvement of TRT (Sun et al., 2023). In this context, the ISOLPHARM project aims to produce radionuclides for nuclear medicine applications at the SPES facility (Selective Production of Exotic Species), making use of the outstanding selection power offered by the Isotope Separation Online (ISOL) technique (Andrighetto et al., 2023, 2019). SPES is under construction at INFN-LNL (National Institute for Nuclear Physics - Legnaro National Laboratories) and is equipped with a cyclotron used to accelerate protons. In the case of the ISOLPHARM project, the beam impinges on a uranium carbide target (primary target), leading to nuclear fission reactions that produce a wide gamma of neutron-rich isotopes, among which ^{111}Ag (Lilli et al., 2023). In order to select the desired species, two selection processes occur. First, a Resonant Ionization Laser Ion Source (RILIS) maximizes the extraction of a specific element from the ion source. Second, a mass spectrometer selects only isotopes with a specific mass within the accelerated Radioactive Ion Beam (RIB). At the end of the beamline, a highly pure beam of a specific radioisotope is collected on a secondary target. After chemical and physical processes, the radionuclides of interest are extracted and used to label proper biological vectors (Ballan et al., 2021).

The ISOLPHARM project focuses on ^{111}Ag, an innovative radionuclide that could be produced at SPES in larger quantities than traditional irradiation-based production (Tosato et al., 2020; Borgna et al., 2017). The properties of this radioisotope may be exploited for theranostic use in nuclear medicine. In fact, ^{111}Ag shows medium energy β-emission and low energy γ-ray emission, suitable for monitoring the delivered dose (Andrighetto et al., 2019; Ballan et al., 2020). ^{111}Ag has a half-life of 7.45 days, similar to ^{177}Lu which is used in radiopharmaceuticals approved by the Food and Drug Administration (FDA) and the European Medicines Agency (EMA) in 2022 (Hennrich and Eder, 2022). Hence, ^{111}Ag properties will be investigated in future preclinical studies within the context of the third experiment promoted by the ISOLPHARM collaboration, ADMIRAL, which extends over a three-year period (2023–2025) (Arzenton, 2023). In order to assess the effects of a ^{111}Ag-based radiopharmaceutical, biodistribution analyses in an *in vivo* model are required. In the context of the ISOLPHARM project, previous studies have been performed to evaluate the biodistribution of a complex containing ^{64}Cu in mouse models, showing promising results (Giaccone et al., 2022; Benfante et al., 2022; Tosato et al., 2022).

The purpose of this study is to investigate a fast and reliable method to localize and quantify ^{111}Ag activity for upcoming preclinical studies. In order to achieve this purpose, imaging tests of aqueous $^{111}Ag^{+}$ solution in calibration phantoms were performed. Images were acquired with Cerenkov Luminescence Imaging (CLI) and digital autoradiography (ARG). CLI is a cheaper and faster alternative to standard nuclear imaging technique for shallow imaging depths, as in the case of small animal studies planned within the ISOLPHARM collaboration (Bhatt et al., 2018; Mc Larney et al., 2021). In fact, CLI offers a valid tool to image β^{-}-emitting radioisotopes such as ^{111}Ag. Several works demonstrated the possibility of performing *in vivo* imaging studies with this optical method, using nuclear medicine probes (Robertson et al., 2009; Ruggiero et al., 2010). However, due to the limited penetration depth of optical photons, CLI is mainly limited to the preclinical scenario, even though some clinical tests have shown promising results (Mc Larney et al., 2021). Nevertheless, future clinical imaging with ^{111}Ag will be based on highly penetrating gamma radiation, exploited by scintigraphy and SPECT. In our study, digital autoradiography was used to obtain γ-ray imaging of ^{111}Ag. It is a consolidated technique that can be used as a control and is based on the scintillation phenomenon as in the case of scintigraphy/SPECT (Solon, 2015; Miller, 2018). The analyses were completed through the development and refinement of a simulation tool, to aid the interpretation of the obtained images. The same experiments have been performed using ^{68}Ga, a positron emitter commonly used in nuclear medicine, to compare newly acquired ^{111}Ag data with a well-known probe.

2. Material and methods

2.1. Radioisotopes

^{111}Ag is a radionuclide with a half-life of 7.45 days. It decays emitting electrons with an average energy of 360 keV and two γ-rays with energy of 342 keV (6.7% intensity) and 245 keV (1.2% intensity) (Morselli et al., 2023). TRT can benefit from the medium energy β emission (Handbook, 2011). Moreover, the contemporary emission of γ-rays makes ^{111}Ag a candidate for theranostic purposes.

Currently, this radionuclide is produced with the standard neutron capture reaction on a palladium target in the TRIGA Mark II nuclear reactor at LENA laboratories in Pavia, where irradiation tests to assess the feasibility of ^{111}Ag production were conducted in the past years (Morselli et al., 2023). For the purpose of the present work, 500 mg of natural palladium were irradiated for 8 h in the central thimble of the reactor; a subsequent dissolution and reformulation process was used to obtain the aqueous solution containing $^{111}Ag^{+}$ that was delivered to the Center for Advanced Preclinical *in vivo* Research (CAPiR) laboratories of Catania University (Tosato et al., 2023).

Instead, the ^{68}Ga solution was supplied by the Cannizzaro Hospital, where it is routinely obtained by a ^{68}Ge/^{68}Ga generator for clinical practice. ^{68}Ga emits positrons with an average energy of 836 keV (Benfante et al., 2023), followed by the emission of two γ-rays resulting from an annihilation process and both having an energy of 511 keV. Table 1 summarizes the physical characteristics of the two radioisotopes discussed in this manuscript.

Table 1
Radioactive decay features of ^{68}Ga and ^{111}Ag.

Isotope	Half-life	Type	Mean energy (keV)	Intensity (%)
^{68}Ga	68 m	$\beta+$	836	88
		γ	511	178
^{111}Ag	7 d	$\beta-$	360	92
		γ	342	7

2.2. Imaging acquisition system

The images were acquired using a Bruker In-Vivo Xtreme, an optical and planar imaging system available for small animals and cell lines. This device is capable of performing multimodal imaging analyses, including Bioluminescence Imaging (BLI), Multispectral VIS-NIR Fluorescence Imaging (MS-FLI), Direct Radioisotopic Imaging (DRI), CLI and X-ray Imaging. DRI is the proprietary name for ARG, the former one will be used in the context of this work (Alitalo et al., 2020; Vizard et al., 1998).

The instrument is based on a reverse detection platform, with an optical system placed underneath the sample support focusing the optical photons onto a 4 MP back-thinned CCD camera. While BLI, FLI and CLI are based on the light produced within the sample itself, DRI and X-ray imaging are achieved using a scintillator plate that converts high-energy radiation into visible and near-visible photons.

The instrument is equipped with different animal chambers and beds. Anesthesia and evacuation systems provide the possibility of performing *in vivo* studies ensuring optimum animal care and end-user safety. Furthermore, the acquisition is managed by a software package, Bruker Molecular Imaging (BMI) version 7.5.2.22464, which allows the modification of acquisition parameters, including illumination, excitation and emission filters, field of view (FOV) and camera exposure times. Even though the present study is based on the use of phantoms, these features will become crucial in the upcoming *in vivo* experiments with mice models and ^{111}Ag.

2.3. Phantoms

The phantoms were custom made with a design based on the Jaszczak one (Jaszczak, 1985). They were composed of one set of three equally deep parallel hollow rods with uniform cross sections. Each hole was placed in such a way that the closest distance between two of them was exactly their diameter. Three different models were produced by the LNL workshop, with cylinders having diameters of 2, 3 and 5 mm. A fourth model was included with a different diameter for each of the three holes. The controlled geometry of the phantom was an advantage, enabling a more precise and accurate quantitative analysis of the collected images. The phantoms were made of PMMA, a transparent material that allowed Cerenkov photons to escape the phantom volume. Fig. 1 shows the top and lateral views of a schematic phantom with 3 mm holes.

2.4. LBC detector

The LBC detector is made of a Scionix LaBrCl(Ce) scintillator and a Hamamatsu PMT model R6231-100-01, optically coupled through an ELJEN Technology EJ-560 silicone rubber band (Morselli et al., 2023). A 3D printed plastic case protects the scintillator and the PMT. The output signal from the detector is read by a CAEN DT-5725SB digitizer. High Voltage is provided by a CAEN DT547N module through the custom made CAENHV_CTRL software. Data acquisition is managed by open source ABCD (Acquisition and Broadcast of Collected Data) software (Fontana et al., 2018). The activity of a sample can be measured through the acquisition of a gamma spectrum with the LBC detector using the equation:

$$A = \frac{N}{\epsilon I_\gamma \Delta t} \quad (1)$$

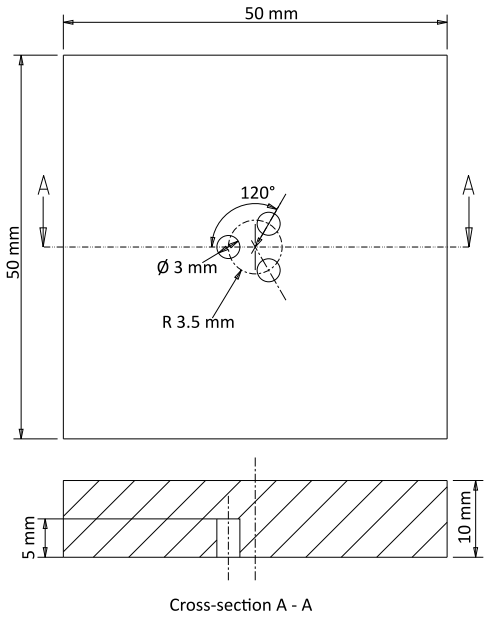

Fig. 1. Phantom design scheme.

where N is the number of counts under the peak associated with a specific transition, ϵ is the absolute photopeak detection efficiency, I_γ is the relative gamma intensity of the considered transition and Δt is the acquisition time in seconds. N is obtained fitting the peak of interest (342 keV for ^{111}Ag and 511 keV for ^{68}Ga), while ϵ is obtained from a simulation developed during the commissioning of the instrument.

2.5. Experimental protocol

At the beginning of the experiment, the $^{111}Ag^{+}$ and $^{68}Ga^{3+}$ stock solutions measured 15.3 MBq and 247 MBq in volumes of 4.7 mL and 5 mL respectively. Both radioactive solutions were kept in screened vials. The activity of the radioactive solutions was measured through the LBC detector, with a source to detector distance of 10 cm.

A micropipette was used to fill the holes of the phantoms with the specific solution. The volume of solution inserted was determined by the diameter of the holes. Holes of 2, 3, and 5 mm were filled with 10, 30, and 75 μL, respectively. The total activity for these volumes can be found in Table 2. Then, the phantoms were covered in plastic wrap and placed in the Bruker In-Vivo Xtreme to acquire the images. Inside the imaging cabinet there is a sample holder consisting of a transparent plastic layer where the phantoms were placed with the holes facing up. A total of four phantoms, one for each of the models described above, was used in the image acquisitions, placing them at the center of the detection plane. A scheme of the used setup is shown in Fig. 2. All the CLI and DRI images were acquired through the BMI software, using the native 1 × 1 binning for the CCD sensor and saving them in Digital Imaging and Communications in Medicine (DICOM) format.

Alongside the image acquisitions, the activity of each phantom was estimated considering the measured activity per milliliter and the injected volume. A correlation between the collected light and the activity content inside the phantom holes was sought for each imaging method.

2.6. Monte-Carlo simulations

Monte Carlo simulations were developed to support the analysis, as well as to provide useful information for upcoming *in vivo* studies. The simulations were built upon Geant4 version 11.0.0 (Allison et al., 2016), a free software package used to accurately simulate the passage

Table 2
Activity of ^{68}Ga and ^{111}Ag according to the hole diameter at the start of the experiment.

Isotope	10 µL	30 µL	75 µL
^{68}Ga	362 kBq	1.1 MBq	2.7 MBq
^{111}Ag	31 kBq	94 kBq	236 kBq

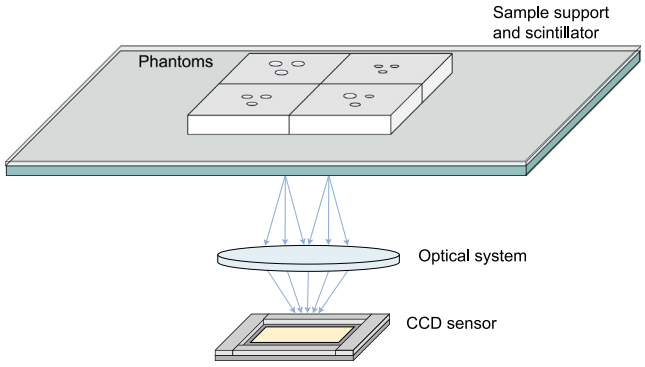

Fig. 2. Scheme of the geometry used in the data collection. The scintillator, represented by the green screen below the sample support, is only present in DRI acquisition mode.

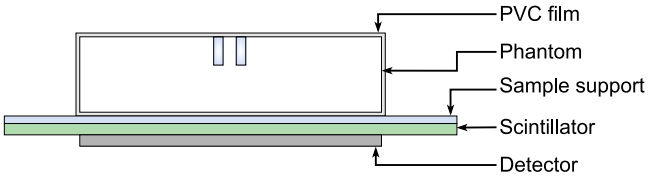

Fig. 3. Scheme of the geometry used in the simulations.

of particles through matter. Every aspect of a physics experiment can be simulated with this toolkit: the geometry of the system, the materials involved, the generation of primary particles, the tracking of particles through materials and many others. Geant4 also offers efficient event and track storage, volumes and particle trajectory visualization on a Graphical User Interface (GUI), alongside data analysis capabilities through its interface with ROOT software (Brun and Rademakers, 1997). Developed in C++, the toolkit uses its object-oriented methodology. The default classes available in the Geant4 toolkit are ready to work but they are also designed to be extended by the user according to their needs. Simulations were based on a schematic setup similar to that shown in Fig. 3. It consisted of a PMMA phantom with holes filled with water, a protective film and a sample holder in PVC, a Gd_2O_2S scintillating screen and a silicon detector. The optical system to focus photons onto the sensor was not modeled, as the internal structure of the Bruker In-Vivo Xtreme was unknown. Therefore, the detector was placed directly in contact with the scintillator (DRI) or with the sample support (CLI). The physics lists employed in the developed simulations are G4EmStandardPhysics_option4, G4OpticalPhysics, G4DecayPhysics and G4RadioactiveDecayPhysics.

The primary particles were the nuclei of interest, namely ^{111}Ag and ^{68}Ga. They were generated at rest and left to decay, thanks to the use of the radioactive decay physics list. The generation and propagation of optical photons were enabled by the optical photon physics lists, which required each material to be assigned a refractive index.

3. Results and discussion

3.1. Cerenkov Luminescence imaging

CLI images were acquired filling one phantom per kind with the radioactive solutions. As an example, Fig. 4 shows the CLI image with ^{111}Ag and ^{68}Ga, obtained with an exposure of 10 and 3 min, respectively, placing all the phantoms inside the instrument.

Table 3
Linear coefficients of the fits in the form $y = mx + q$ for ^{68}Ga and ^{111}Ag CLI images.

Isotope	m (kBq^{-1}s^{-1})	q (s^{-1})
^{68}Ga	21.8	−1690
^{111}Ag	4.71	1.73

In both images, all the holes are recognizable, implying a resolution of at least 2 mm for the CLI method with the two used radionuclides. However, there are two main noticeable differences: the image with ^{111}Ag features sharper edges, indicating higher resolution, but the counts are significantly reduced despite approximately three times longer acquisition time. Both facts can be attributed to the different energy spectra of the β particles produced by the decay of the radionuclides themselves. With a lower average energy compared to ^{68}Ga positrons, ^{111}Ag electrons travel shorter distances within the material. This results in smaller and more localized light production (Ciarrocchi and Belcari, 2017). Furthermore, the ^{68}Ga activity was approximately 5 times higher than that of ^{111}Ag at the time of acquisition.

Images were analyzed to search for a correlation between the collected light and activity in order to assess quantitative information from the images in view of future experiments. The structure of the images, with light organized in clusters corresponding to different holes, suggested the use of clustering algorithms such as Density-Based Spatial Clustering of Applications with Noise (DBSCAN) (Ester et al., 1996). However, the current algorithm could not be directly applied to images conceived as 2D histograms with non-binary bin contents.

Indeed, DBSCAN operates by evaluating point density, which is constant in a 2D histogram because each pixel is surrounded by a fixed number of pixels (excluding borders). Instead, in the present study, discrimination had to be based on the pixels' value, considering a cluster as a group of pixels exhibiting higher counts than their immediate neighbors. Therefore, the images were preprocessed as follows: a threshold was set for the pixel content and, starting from a white canvas, a point was drawn at the coordinates of a pixel only if its value was greater than the chosen lower threshold. Thus, a new image was obtained in which points were drawn in correspondence of high-valued pixels, making clusters of points emerge where groups of pixels boasting elevated values were present. DBSCAN algorithm could then be applied to the pre-processed images and several quantities related to light intensity were estimated for each identified cluster. Afterwards, possible correlations between these quantities and the sample activity were sought.

The activity content of each hole was estimated as $A = V \cdot A_{\mathrm{ml}}$, where V was the volume of solution placed in each hole and A_{ml} was the activity per milliliter of $^{111}Ag^{+}$ (or $^{68}Ga^{3+}$) solution at the time of image acquisition. This last quantity was obtained from the activity measurements of the radioactive solution with the LBC detector, taking into account the decay of the radionuclide in the time interval between the initial activity estimation and the image acquisition.

The quantity most strongly correlated with the radioactive activity was the total light output, calculated by summing the pixel counts around the center of the cluster within 1.5 times the radius of the holes themselves. Both Cerenkov-based images with ^{111}Ag and ^{68}Ga yielded the same conclusions. To remove the dependence of the counts on the acquisition time, they were normalized to the latter, resulting in counts per second. Fig. 5 shows the relationship between counts per second and activity for CLI data obtained with ^{111}Ag and ^{68}Ga. A linear fit was also performed to highlight the linear correlation between the two quantities. Linear coefficients are presented in Table 3.

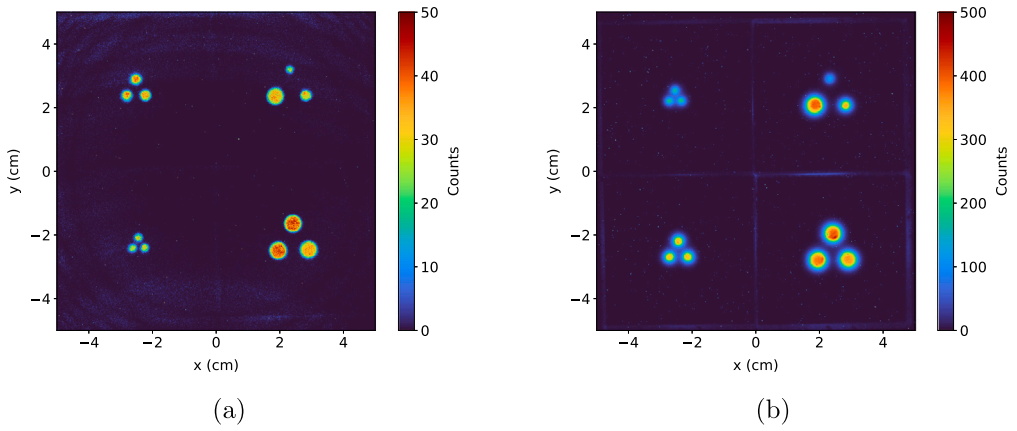

Fig. 4. CLI images with ^{111}Ag (a) and ^{68}Ga (b). For the ^{111}Ag image, phantoms' diameters are 3 mm at top-left, mixed at top-right, 2 mm at bottom-left, 5 mm at bottom-right. For the ^{68}Ga image, phantoms' diameters are 2 mm at top-left, mixed at top-right, 3 mm at bottom-left, 5 mm at bottom-right.

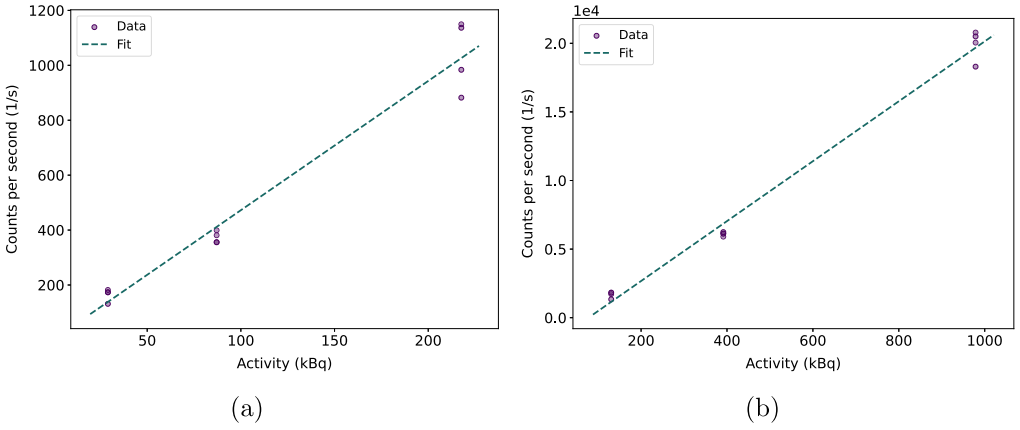

Fig. 5. Correlation plot counts per second vs activity for each cluster in the ^{111}Ag (a) and ^{68}Ga (b) CLI experimental image, dashed lines are linear fits.

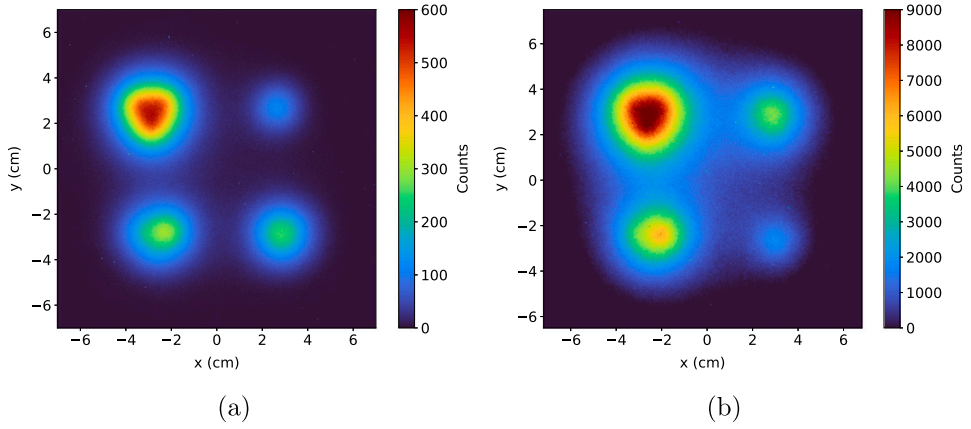

Fig. 6. DRI images with ^{111}Ag (a) and ^{68}Ga (b). For the ^{111}Ag image, phantoms' diameters are 5 mm at top-left, 2 mm at top-right, mixed at bottom-left, 3 mm at bottom-right. For the ^{68}Ga image, phantoms' diameters are 5 mm at top-left, 3 mm at top-right, mixed at bottom-left, 2 mm at bottom-right.

3.2. Direct radioisotopic imaging

The same experimental procedure was performed for the DRI images, acquiring data with a phantom of each kind placed inside the imaging cabinet. Fig. 6 shows the experimental images obtained with ^{111}Ag and ^{68}Ga and an exposure time of 5 min and 30 s respectively.

A relevant difference with respect to the CLI case is that the holes inside a single phantom are not distinguishable. Electrons of 360 keV have a mean CSDA range of approximately 1 mm in PMMA (Seltzer, 1993), meaning that only γ-rays coming from ^{111}Ag decay can travel through the 5 mm thickness of PMMA separating the bottom of the holes and the scintillator screen. The same applies to the positrons generated in ^{68}Ga decay. Hence DRI images are caused only by the γ-rays interacting with the scintillator plate. Considering the isotropic emission of such particles and the fact that most of them travel PMMA unperturbed, scintillation can take place far away from the radioactive

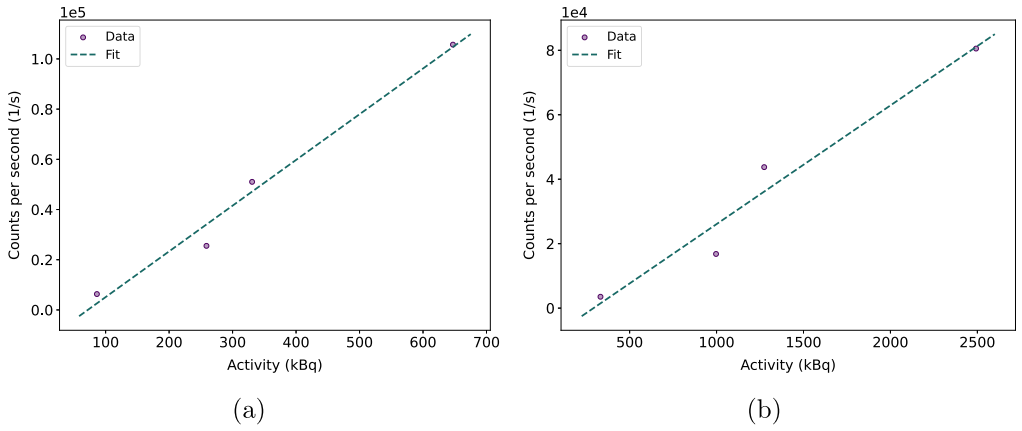

Fig. 7. Correlation plot counts per second vs activity for each cluster in the ^{111}Ag (a) and ^{68}Ga (b) DRI experimental image. Dashed lines are linear fits.

Table 4
Linear coefficients of the fits in the form $y = mx + q$ for ^{68}Ga and ^{111}Ag DRI images.

Isotope	m (kBq^{-1}s^{-1})	q (s^{-1})
^{68}Ga	36.83	−10760
^{111}Ag	182.1	−13090

decay vertex. As a result, the distribution of light is widened with respect to the CLI case, where light production occurs only close to the decay point.

As in the case of the CLI images, the DBSCAN algorithm was used to identify the light clusters and estimate different quantities searching for a light-activity correlation. Once again, the total light yield was the most correlated for both ^{111}Ag and ^{68}Ga data. Fig. 7 shows the plot of counts per second - activity for the DRI ^{111}Ag and ^{68}Ga images. Linear coefficients are presented in Table 4.

In conclusion, data analysis demonstrated the possibility of retrieving quantitative information from experimental images, showcasing the potential for establishing a correlation between the counts and radionuclide activity in CLI and DRI acquisition modes. This potential will be crucial for the upcoming *in vivo* imaging studies, where the activity in specific organs or regions within a mouse's body will be estimated via CLI and DRI images. To enable such an estimation process, the analysis had to be integrated by creating a framework that allows for activity quantification regardless of the geometry and the materials of the sample. Simulations were fundamental in achieving this outcome, allowing us to link light intensities across different experimental setups.

3.3. Simulation tuning

For the simulation part of the experiment, a simplified configuration was used due to the unknown internal structure of the actual instrument. The detector was positioned in contact with either the scintillating screen (for DRI) or the sample support (for CLI). To ensure the reliability of the simulation tool, the latter was tuned using experimental data, devising simulation strategies for both imaging methods. This fine-tuning involved adjusting unknown parameters while comparing simulated and experimental images using clusters' profiles. By selecting a region of interest (ROI) around the center of each hole, a profile along the x-axis was obtained by summing the pixels vertically. The profiles were compared with respect to their shape and the relative intensity of the different holes, which needed to be consistent with the experimental images. Fig. 8 depicts the CLI image with ^{111}Ag on the left, highlighting the centers of various clusters and the associated regions of interest. The right panel, instead, shows the profiles of the different clusters for the considered image.

To obtain CLI images that closely resembled the experimental ones, a constraint on the angle of entrance of optical photons in the detector was imposed. In the case of DRI, however, this was not necessary; the unknown parameter to be tuned was the scintillator thickness. Moreover, the optical photon absorption length for radioactive solutions had to be derived from the comparison of profiles between experimental and simulated images since these parameters were not known in advance.

Fig. 9 shows the experimental CLI image with ^{111}Ag (left) and the corresponding simulated image (right). Fig. 10 shows, instead, a comparison of all the profiles hole by hole, for the two images.

Once a reliable simulation tool was developed, it was used to asses quantitative information about the imaging modalities, like spatial resolution.

3.4. Spatial resolution

One of the most common ways of measuring the spatial resolution of an imaging system in nuclear medicine is the point spread function (PSF), particularly its full width at half maximum (FWHM) and full width at tenth maximum (FWTM) (Bailey, 2015). Using the developed simulations, it was possible to model a point-like source inside a phantom to obtain the PSF. The source was positioned at the geometrical center of a uniform PMMA phantom with dimensions equal to the ones used in the real experiments. It was thus possible to retrieve the PSF of ^{111}Ag and ^{68}Ga, in both acquisition modes.

To obtain the FWHM and the FWTM, the center of the PSFs were fitted with a parabola in order to obtain the maximum height. Then, the half maximum and tenth maximum locations were determined by linear interpolations from the nearest two neighboring points of the half and tenth peak value, as described in the NEMA NU 1-2018 guidelines (NEMA, 2019). Fig. 11 shows the PSF, the FWHM and the FWTM for ^{111}Ag and ^{68}Ga in CLI mode. The results of the analysis are presented in Table 5.

^{111}Ag appears to be characterized by a better spatial resolution than ^{68}Ga for both imaging methods. Although the FWHM values are similar, the difference can be noticed with the FWTM. In fact, due to the shape of the PSF, which broadens more below half of the maximum, the difference between the two radionuclides becomes more apparent using the width at tenth maximum.

Given that typical resolution values for a SPECT system are around 2 mm (Attarwala et al., 2020), the FWHM values obtained highlight the potential of CLI and DRI for preclinical imaging. Moreover, since tumors in mice can be considered macroscopic when they reach a diameter of at least 2 mm (Puaux et al., 2011), it should be possible to distinguish such structures using the imaging methods applied, especially CLI. However, unlike SPECT imaging, it is important to note that the spatial resolution of a CLI system is heavily influenced by the optical properties of the medium where the source is located, and even more so by the depth of the source. Regarding DRI, due to the absence

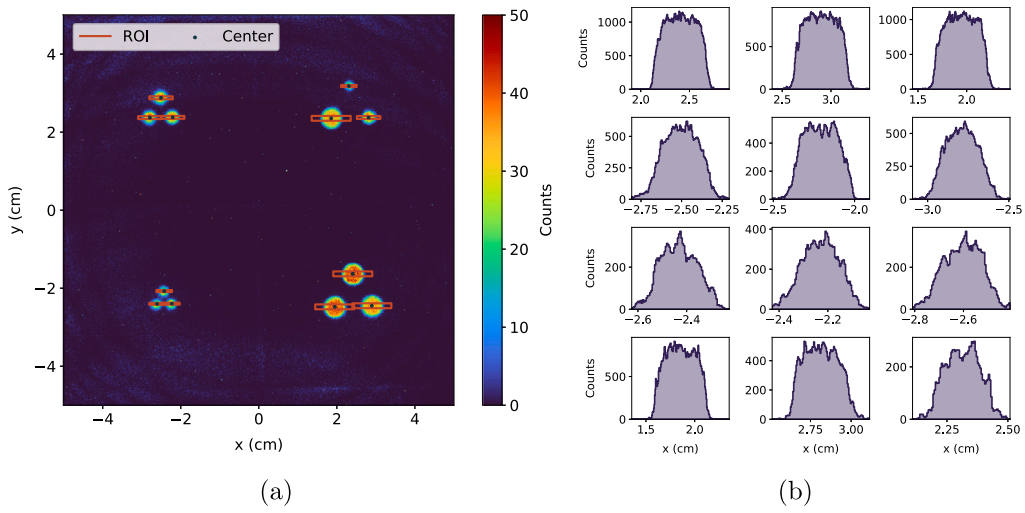

Fig. 8. Analysis of CLI image with ^{111}Ag. Identification of the cluster centers marked as blue dots and the regions of interest shown with red lines (a). Profiles obtained for each cluster (b).

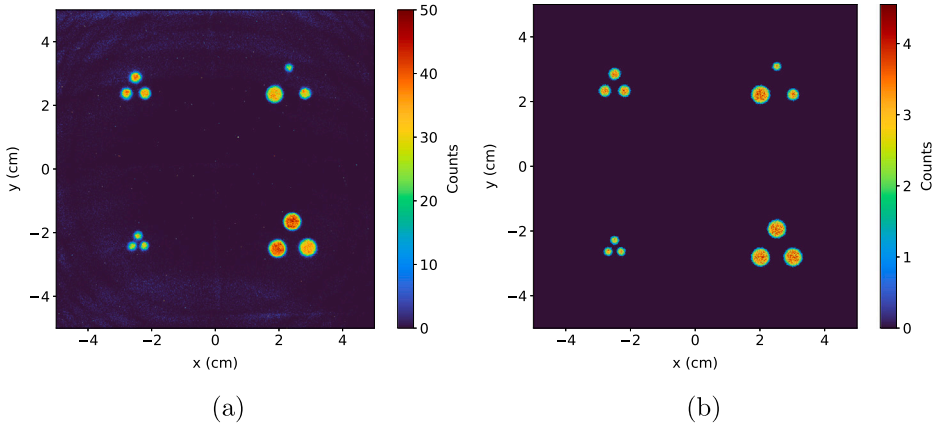

Fig. 9. ^{111}Ag CLI experimental (a) and simulated (b) images.

Table 5
FWHM and FWTM of ^{111}Ag and ^{68}Ga with the two imaging methods, CLI and DRI.

Isotope	CLI		DRI	
	FWHM (mm)	FWTM (mm)	FWHM (mm)	FWTM (mm)
^{68}Ga	0.5	1.6	3.5	11
^{111}Ag	0.4	0.9	2.2	8.4

of a collimation system, increasing the source-to-scintillator distance causes a substantial broadening of the PSF, leading to a detrimental effect on spatial resolution. As a result, the above findings cannot be generalized to any geometric configuration and are only applicable at shallow depths, both for CLI and DRI.

Eventually, a simulation tool able to mimic experimental data was obtained. Although some properties like spatial resolution were estimated, the developed software will be particularly useful for analyzing, planning, and optimizing future experiments prior to data collection. Furthermore, the simulation tool will have a crucial role in performing quantitative analysis for upcoming *in vivo* studies. The MOBY digital mouse model (Carter et al., 2019; Segars et al., 2004) will be included in the simulations to ensure a better quantitative interpretation of preclinical data. In addition, this expedient will allow us to reduce the number of animal tests, still obtaining valuable insights on the new radiopharmaceutical. Preliminary simulated images have already been obtained using MOBY, however its potential will be fully exploited in the near future, through the comparison with preclinical data on mice models.

4. Conclusions

TRT is a consolidated approach for cancer treatments that provides advantages over other modalities. In fact, the selectivity of this technique enables the exertion of the cytotoxic effect predominantly on tumor cells, preserving healthy tissue from the radiation-induced damage. TRT developments are focused on the enhancement of the efficacy of this form of treatment, studying innovative vectors, new labeling techniques and radionuclides that may be used to synthesize novel radiopharmaceuticals (Sgouros et al., 2020).

In the present work, the characterization of CLI and DRI scans is presented together with a preliminary imaging study regarding ^{111}Ag. The valuable properties of ^{111}Ag for TRT captured the interest of the ISOLPHARM collaboration. In fact, the emission of both electrons and γ-rays makes ^{111}Ag a good candidate for theranostic applications in TRT (Andrighetto et al., 2019). Specifically, in our study, the Bruker In-Vivo Xtreme device was selected to perform preliminary imaging scans and pave the way for preclinical imaging investigation. ^{111}Ag was examined in phantoms, providing valuable insights for the upcoming *in vivo* studies. The success in obtaining accurate images highlighted the theranostic potential of ^{111}Ag, building the rationale for future biodistribution experiments in mice models using ^{111}Ag-labeled radiopharmaceuticals. Furthermore, the possibility of retrieving quantitative

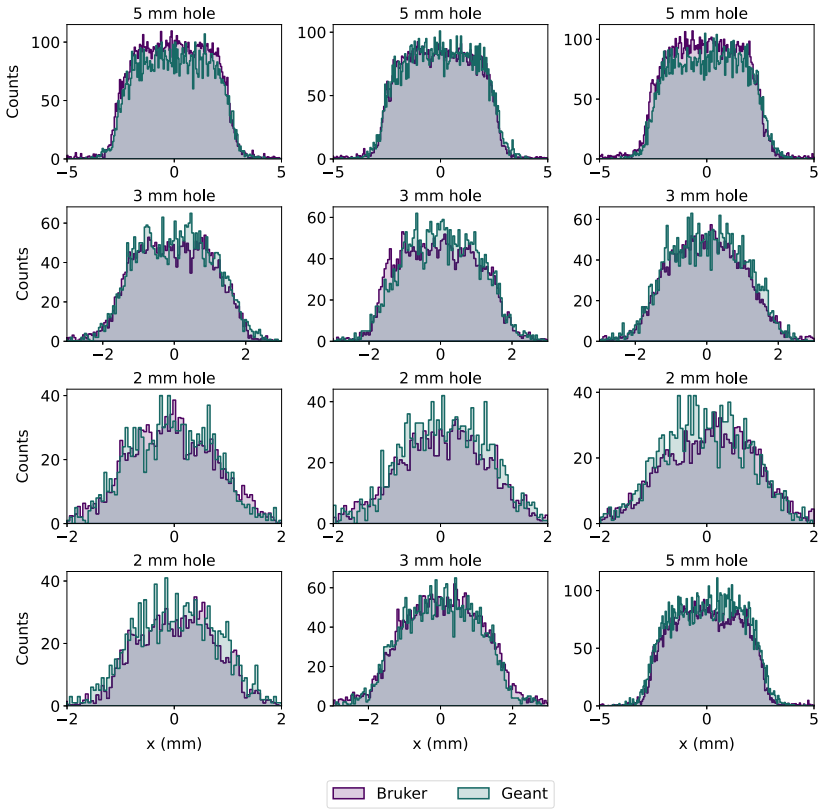

Fig. 10. Comparison of experimental and simulated profiles for ^{111}Ag CLI images.

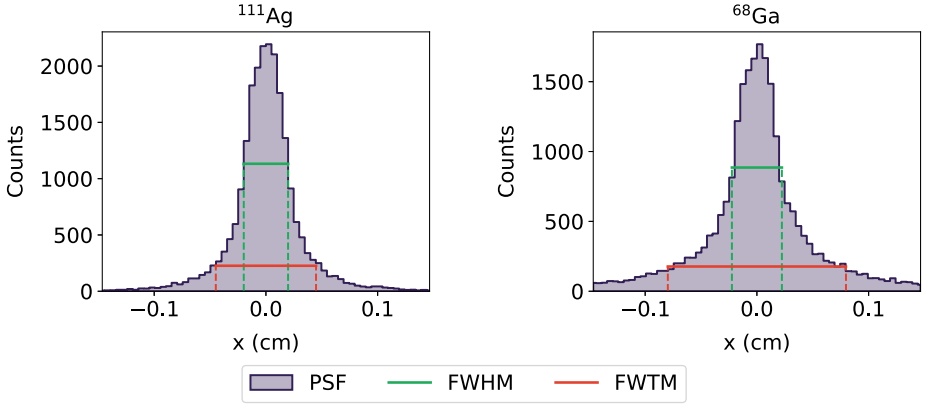

Fig. 11. Point spread functions of ^{111}Ag (left) and ^{68}Ga for CLI mode. The point source was placed in the center of a uniform PMMA phantom like the ones used in the experimental setup. FWHM and FWTM are highlighted with colored lines and their values are presented in Table 5.

information from CLI and DRI images was investigated. The analysis revealed a relation between the intensity of the collected light and the activity of the sample. To generalize the analysis, Monte Carlo simulations based on Geant4 toolkit were built to develop a quantitative framework that could work with several experimental setups, as in the case of future *in vivo* studies with mice models. To pursue such an objective, simulations were tuned with experimental data performing a comparison of light profiles between experimental and simulated images. The development of a reliable simulation tool validated with CLI and DRI images of calibration phantoms lays the foundation for the future studies foreseen by the ISOLPHARM collaboration. Moreover, integrating the MOBY digital mouse model (Segars et al., 2004) in the software will aid the quantitative analysis of the upcoming *in vivo* images that will be collected, making it possible to investigate the theranostic potential of ^{111}Ag in a preclinical scenario.

CRediT authorship contribution statement

Davide Serafini: Writing – review & editing, Writing – original draft, Visualization, Validation, Software, Methodology, Investigation, Formal analysis, Data curation, Conceptualization. **Nicola Zancopè:** Writing – review & editing, Writing – original draft, Visualization, Validation, Software, Methodology, Investigation, Formal analysis, Data curation, Conceptualization,. **Anna Maria Pavone:** Writing – review & editing, Writing – original draft, Visualization, Validation, Methodology, Investigation, Data curation, Conceptualization. **Viviana Benfante:** Writing – review & editing, Visualization, Validation, Methodology, Investigation. **Alberto Arzenton:** Writing – review & editing, Visualization, Validation, Methodology, Investigation. **Vincenzo Russo:** Visualization, Validation, Methodology, Investigation. **Michele Ballan:** Visualization, Resources. **Luca Morselli:** Visualization, Resources,

Methodology. **Francesco Paolo Cammarata:** Visualization, Supervision, Resources, Methodology, Investigation, Conceptualization. **Albert Comelli:** Visualization, Supervision, Methodology, Investigation. **Giorgio Russo:** Writing – review & editing, Visualization, Supervision, Resources, Methodology, Investigation, Conceptualization. **Fabrizio Scopelliti:** Visualization, Resources. **Valerio Di Marco:** Writing – review & editing, Visualization, Supervision, Resources. **Francesca Mastrotto:** Visualization, Supervision, Resources. **Mattia Asti:** Writing – review & editing, Visualization. **Devid Maniglio:** Writing – review & editing, Visualization, Resources. **Carla Sbarra:** Writing – review & editing, Visualization, Resources. **Silva Bortolussi:** Writing – review & editing, Visualization, Resources. **Antonietta Donzella:** Writing – review & editing, Visualization, Resources. **Aldo Zenoni:** Visualization, Resources. **Andrea Gandini:** Visualization, Resources. **Valerio Villa:** Visualization, Resources. **Diego Paderno:** Visualization, Resources. **Lisa Zangrando:** Visualization, Software, Resources. **Stefano Corradetti:** Visualization, Resources. **Emilio Mariotti:** Writing – review & editing, Visualization, Resources. **Andrea Salvini:** Visualization, Resources. **Filippo Torrisi:** Visualization, Resources. **Marcello Lunardon:** Writing – review & editing, Visualization, Supervision, Resources, Methodology, Conceptualization. **Alberto Andrighetto:** Visualization, Supervision, Resources, Project administration, Funding acquisition, Conceptualization.

Declaration of competing interest

The authors declare that they have no known competing financial interests or personal relationships that could have appeared to influence the work reported in this paper.

Acknowledgments

This research is part of the ADMIRAL experiment that is supported by the INFN, Italy. The authors thank the LNL workshop staff for their technological support.

Data availability

Data will be made available on request.

References

Alitalo, O., Rantamäki, T., Huhtala, T., 2020. Digital autoradiography for efficient functional imaging without anesthesia in experimental animals: Reversing phencyclidine-induced functional alterations using clozapine. Prog. Neuro-Psychopharmacol. Biol. Psychiatry 100, 109887. http://dx.doi.org/10.1016/j.pnpbp.2020.109887.

Allison, J., Amako, K., Apostolakis, J., Arce, P., Asai, M., Aso, T., Bagli, E., Bagulya, A., Banerjee, S., Barrand, G., Beck, B., Bogdanov, A., Brandt, D., Brown, J., Burkhardt, H., Canal, P., Cano-Ott, D., Chauvie, S., Cho, K., Cirrone, G., Cooperman, G., Cortés-Giraldo, M., Cosmo, G., Cuttone, G., Depaola, G., Desorgher, L., Dong, X., Dotti, A., Elvira, V., Folger, G., Francis, Z., Galoyan, A., Garnier, L., Gayer, M., Genser, K., Grichine, V., Guatelli, S., Guèye, P., Gumplinger, P., Howard, A., Hřivnáčová, I., Hwang, S., Incerti, S., Ivanchenko, A., Ivanchenko, V., Jones, F., Jun, S., Kaitaniemi, P., Karakatsanis, N., Karamitros, M., Kelsey, M., Kimura, A., Koi, T., Kurashige, H., Lechner, A., Lee, S., Longo, F., Maire, M., Mancusi, D., Mantero, A., Mendoza, E., Morgan, B., Murakami, K., Nikitina, T., Pandola, L., Paprocki, P., Perl, J., Petrović, I., Pia, M., Pokorski, W., Quesada, J., Raine, M., Reis, M., Ribon, A., Ristić Fira, A., Romano, F., Russo, G., Santin, G., Sasaki, T., Sawkey, D., Shin, J., Strakovsky, I., Taborda, A., Tanaka, S., Tomé, B., Toshito, T., Tran, H., Truscott, P., Urban, L., Uzhinsky, V., Verbeke, J., Verderi, M., Wendt, B., Wenzel, H., Wright, D., Wright, D., Yamashita, T., Yarba, J., Yoshida, H., 2016. Recent developments in Geant4. Nucl. Instrum. Methods Phys. Res. A 835, 186–225. http://dx.doi.org/10.1016/j.nima.2016.06.125, URL https://www.sciencedirect.com/science/article/pii/S0168900216306957.

Andrighetto, A., Centofante, L., Gramegna, F., Monetti, A., Ballan, M., Zenoni, A., Corradetti, S., Lilli, G., Manzolaro, M., Marchi, T., Arzenton, A., Khwairakpam, O., Scarpa, D., Donzella, A., Mariotti, E., Meneghetti, G., Colombo, P., Biasetto, L., Oboe, R., Lunardon, M., Rifuggiato, D., 2023. Low energy radioactive ion beams at SPES for nuclear physics and medical applications. Nucl. Instrum. Methods Phys. Res. B 541, 236–239. http://dx.doi.org/10.1016/j.nimb.2023.05.044, URL https://www.sciencedirect.com/science/article/pii/S0168583X23002458.

Andrighetto, A., Tosato, M., Ballan, M., Corradetti, S., Borgna, F., Di Marco, V., Marzaro, G., Realdon, N., 2019. The ISOLPHARM project: ISOL-based production of radionuclides for medical applications. J. Radioanal. Nucl. Chem. 322 (1), 73–77. http://dx.doi.org/10.1007/s10967-019-06698-0.

Arzenton, A., 2023. Radiobiological model for β-emitter radiopharmaceutical therapy in dynamic cell cultures in the framework of the ISOLPHARM project. Il Nuovo Cimento C 46 (3), 1–10. http://dx.doi.org/10.1393/ncc/i2023-23072-3.

Attarwala, A.A., Hardiansyah, D., Romanó, C., Jiménez-Franco, L.D., Roscher, M., Wängler, B., Glatting, G., 2020. Performance assessment of the albira ii preclinical spect s102 system for 99mtc imaging. Ann. Nucl. Med. 35 (1), 111–120. http://dx.doi.org/10.1007/s12149-020-01547-7.

Bailey, D.L. (Ed.), 2015. International atomic energy agency. In: Nuclear Medicine Physics. IAEA, Vienna, Austria.

Ballan, M., Tosato, M., Verona, M., Caeran, M., Borgna, F., Vettorato, E., Corradetti, S., Zangrando, L., Sgaravatto, M., Verlato, M., Asti, M., Marzaro, G., Mastrotto, F., Di Marco, V., Maniglio, D., Bisio, A., Motta, A., Quaranta, A., Zenoni, A., Pastore, P., Realdon, N., Andrighetto, A., 2020. Preliminary evaluation of the production of non-carrier added ^{111}Ag as core of a therapeutic radiopharmaceutical in the framework of ISOLPHARM_Ag experiment. Appl. Radiat. Isot. 164, 109258. http://dx.doi.org/10.1016/j.apradiso.2020.109258, URL https://www.sciencedirect.com/science/article/pii/S0969804320304085.

Ballan, M., Vettorato, E., Morselli, L., Tosato, M., Nardella, S., Borgna, F., Corradetti, S., Monetti, A., Lunardon, M., Zenoni, A., Di Marco, V., Realdon, N., Andrighetto, A., 2021. Development of implantation substrates for the collection of radionuclides of medical interest produced via ISOL technique at INFN-LNL. Appl. Radiat. Isot. 175, 109795. http://dx.doi.org/10.1016/j.apradiso.2021.109795, URL https://www.sciencedirect.com/science/article/pii/S0969804321002001.

Benfante, V., Stefano, A., Ali, M., Laudicella, R., Arancio, W., Cucchiara, A., Caruso, F., Cammarata, F.P., Coronnello, C., Russo, G., Miele, M., Vieni, A., Tuttolomondo, A., Yezzi, A., Comelli, A., 2023. An overview of in vitro assays of ^{64}Cu-, ^{68}Ga-, ^{125}i-, and ^{99m}Tc-labelled radiopharmaceuticals using radiometric counters in the era of radiotheranostics. Diagnostics 13 (7), http://dx.doi.org/10.3390/diagnostics13071210, URL https://www.mdpi.com/2075-4418/13/7/1210.

Benfante, V., Stefano, A., Comelli, A., Giaccone, P., Cammarata, F.P., Richiusa, S., Scopelliti, F., Pometti, M., Ficarra, M., Cosentino, S., Lunardon, M., Mastrotto, F., Andrighetto, A., Tuttolomondo, A., Parenti, R., Ippolito, M., Russo, G., 2022. A new preclinical decision support system based on PET radiomics: A preliminary study on the evaluation of an innovative^{64}Cu-labeled chelator in mouse models. J. Imaging 8 (4), http://dx.doi.org/10.3390/jimaging8040092, URL https://www.mdpi.com/2313-433X/8/4/92.

Bhatt, N.B., Pandya, D.N., Dezarn, W.A., Marini, F.C., Zhao, D., Gmeiner, W.H., Triozzi, P.L., Wadas, T.J., 2018. Practical Guidelines for Cerenkov Luminescence Imaging with Clinically Relevant Isotopes. Springer New York, pp. 197–208. http://dx.doi.org/10.1007/978-1-4939-7860-1_15, Ch. 15.

Borgna, F., Ballan, M., Corradetti, S., Vettorato, E., Monetti, A., Rossignoli, M., Manzolaro, M., Scarpa, D., Mazzi, U., Realdon, N., Andrighetto, A., 2017. A preliminary study for the production of high specific activity radionuclides for nuclear medicine obtained with the isotope separation on line technique. Appl. Radiat. Isot. 127, 214–226. http://dx.doi.org/10.1016/j.apradiso.2017.06.022, URL https://www.sciencedirect.com/science/article/pii/S0969804316309034.

Brosch-Lenz, J., Delker, A., Völter, F., Unterrainer, L.M., Kaiser, L., Bartenstein, P., Ziegler, S., Rahmim, A., Uribe, C., Böning, G., 2023. Toward single-time-point image-based dosimetry of^{177}Lu-PSMA-617 therapy. J. Nucl. Med. 64 (5), 767–774. http://dx.doi.org/10.2967/jnumed.122.264594, arXiv:https://jnm.snmjournals.org/content/64/5/767.full.pdf. URL https://jnm.snmjournals.org/content/64/5/767.

Brun, R., Rademakers, F., 1997. ROOT— An object oriented data analysis framework. Nucl. Instrum. Methods Phys. Res. A 389 (1), 81–86. http://dx.doi.org/10.1016/S0168-9002(97)00048-X, new Computing Techniques in Physics Research V. URL https://www.sciencedirect.com/science/article/pii/S016890029700048X.

Carter, L.M., Crawford, T.M., Sato, T., Furuta, T., Choi, C., Kim, C.H., Brown, J.L., Bolch, W.E., Zanzonico, P.B., Lewis, J.S., 2019. PARaDIM: A PHITS-based monte carlo tool for internal dosimetry with tetrahedral mesh computational phantoms. J. Nucl. Med. 60 (12), 1802–1811. http://dx.doi.org/10.2967/jnumed.119.229013, arXiv:https://jnm.snmjournals.org/content/60/12/1802.full.pdf. URL https://jnm.snmjournals.org/content/60/12/1802.

Ciarrocchi, E., Belcari, N., 2017. Cerenkov luminescence imaging: physics principles and potential applications in biomedical sciences. EJNMMI Phys. 4 (1), http://dx.doi.org/10.1186/s40658-017-0181-8.

Ester, M., Kriegel, H.-P., Sander, J., Xu, X., 1996. A density-based algorithm for discovering clusters in large spatial databases with noise. In: Proceedings of the Second International Conference on Knowledge Discovery and Data Mining. KDD'96, AAAI Press, pp. 226–231.

Fontana, C.L., Carnera, A., Lunardon, M., Pino, F.E., Sada, C., Soramel, F., Stevanato, L., Moretto, S., 2018. A distributed data acquisition system for nuclear detectors. Int. J. Mod. Phys.: Conf. Ser. 48, 1860118. http://dx.doi.org/10.1142/S2010194518601187, arXiv:https://doi.org/10.1142/S2010194518601187.

Giaccone, P., Benfante, V., Stefano, A., Cammarata, F.P., Russo, G., Comelli, A., 2022. PET images atlas-based segmentation performed in native and in template space: A radiomics repeatability study in mouse models. In: Mazzeo, P.L., Frontoni, E., Sclaroff, S., Distante, C. (Eds.), Image Analysis and Processing. ICIAP 2022 Workshops. Springer International Publishing, Cham, pp. 351–361.

2011. Handbook of nuclear chemistry. http://dx.doi.org/10.1007/978-1-4419-0720-2.

Hennrich, U., Eder, M., 2022. ^{177}LuLu-PSMA-617 (Pluvicto^{TM}): The first FDA-approved radiotherapeutical for treatment of prostate cancer. Pharmaceuticals 15 (10), http://dx.doi.org/10.3390/ph15101292, URL https://www.mdpi.com/1424-8247/15/10/1292.

Jaszczak, R.J., 1985. Nuclear imaging phantom. URL https://patents.google.com/patent/US4499375A/en.

Lilli, G., Centofante, L., Manzolaro, M., Monetti, A., Oboe, R., Andrighetto, A., 2023. Remote handling systems for the selective production of exotic species (SPES) facility. Nucl. Eng. Technol. 55 (1), 378–390. http://dx.doi.org/10.1016/j.net.2022.08.034, URL https://www.sciencedirect.com/science/article/pii/S1738573322004326.

Mc Larney, B., Skubal, M., Grimm, J., 2021. A review of recent and emerging approaches for the clinical application of Cerenkov luminescence imaging. Front. Phys. 9, http://dx.doi.org/10.3389/fphy.2021.684196, URL https://www.frontiersin.org/articles/10.3389/fphy.2021.684196.

Miller, B.W., 2018. Radiation imagers for quantitative, single-particle digital autoradiography of alpha- and beta-particle emitters. Semin. Nucl. Med. 48 (4), 367–376. http://dx.doi.org/10.1053/j.semnuclmed.2018.02.008, instrumentation. URL https://www.sciencedirect.com/science/article/pii/S0001299818300163.

Morris, Z.S., Wang, A.Z., Knox, S.J., 2021. The radiobiology of radiopharmaceuticals. Semin. Radiat. Oncol. 31 (1), 20–27. http://dx.doi.org/10.1016/j.semradonc.2020.07.002, Rapid Evolution in Theranostics. URL https://www.sciencedirect.com/science/article/pii/S1053429620300473.

Morselli, L., Donzella, A., Arzenton, A., Asti, M., Bortolussi, S., Corradetti, S., D'Agostino, G., Di Luzio, M., Ferrari, M., Gandini, A., Lunardon, M., Villa, V., Salvini, A., Zangrando, L., Zenoni, A., Andrighetto, A., 2023. Production and characterization of ^{111}Ag radioisotope for medical use in a TRIGA Mark II nuclear research reactor. Appl. Radiat. Isot. 197, 110798. http://dx.doi.org/10.1016/j.apradiso.2023.110798.

2019. NEMA Standards Publication NU 1-2018. National Electrical Manufacturers Association, Rosslyn, Virginia.

Puaux, A.-L., Ong, L.C., Jin, Y., Teh, I., Hong, M., Chow, P.K.H., Golay, X., Abastado, J.-P., 2011. A comparison of imaging techniques to monitor tumor growth and cancer progression in living animals. Int. J. Mol. Imaging 2011, 1–12. http://dx.doi.org/10.1155/2011/321538.

Robertson, R., Germanos, M.S., Li, C., Mitchell, G.S., Cherry, S.R., Silva, M.D., 2009. Optical imaging of Cerenkov light generation from positron-emitting radiotracers. Phys. Med. Biol. 54 (16), N355. http://dx.doi.org/10.1088/0031-9155/54/16/N01.

Rowland, D.J., Cherry, S.R., 2008. Small-animal preclinical nuclear medicine instrumentation and methodology. Semin. Nucl. Med. 38 (3), 209–222. http://dx.doi.org/10.1053/j.semnuclmed.2008.01.004, Developments in Instrumentation. URL https://www.sciencedirect.com/science/article/pii/S0001299808000238.

Ruggiero, A., Holland, J.P., Lewis, J.S., Grimm, J., 2010. Cerenkov luminescence imaging of medical isotopes. J. Nucl. Med. 51 (7), 1123–1130. http://dx.doi.org/10.2967/jnumed.110.076521, arXiv:https://jnm.snmjournals.org/content/51/7/1123.full.pdf. URL https://jnm.snmjournals.org/content/51/7/1123.

Segars, W., Tsui, B.M., Frey, E.C., Johnson, G., Berr, S.S., 2004. Development of a 4-D digital mouse phantom for molecular imaging research. Mol. Imaging Biol. 6 (3), 149–159. http://dx.doi.org/10.1016/j.mibio.2004.03.002, URL https://www.sciencedirect.com/science/article/pii/S1536163204002173.

Seltzer, S., 1993. Stopping-powers and range tables for electrons, protons, and helium ions, NIST standard reference database 124. http://dx.doi.org/10.18434/T4NC7P, URL http://www.nist.gov/pml/data/star/index.cfm.

Sgouros, G., Bodei, L., McDevitt, M.R., Nedrow, J.R., 2020. Radiopharmaceutical therapy in cancer: clinical advances and challenges. Nat. Rev. Drug Discov. 19 (9), 589–608. http://dx.doi.org/10.1038/s41573-020-0073-9.

Solon, E.G., 2015. Autoradiography techniques and quantification of drug distribution. Cell Tissue Res. 360 (1), 87–107. http://dx.doi.org/10.1007/s00441-014-2093-4.

Sun, Q., Li, J., Ding, Z., Liu, Z., 2023. Radiopharmaceuticals heat anti-tumor immunity. Theranostics 13, 767–786. http://dx.doi.org/10.7150/thno.79806, URL https://www.thno.org/v13p0767.htm.

Tosato, M., Asti, M., Dalla Tiezza, M., Orian, L., Häussinger, D., Vogel, R., Köster, U., Jensen, M., Andrighetto, A., Pastore, P., Marco, V.D., 2020. Highly stable silver(i) complexes with cyclen-based ligands bearing sulfide arms: A step toward silver-111 labeled radiopharmaceuticals. Inorg. Chem. 59 (15), 10907–10919. http://dx.doi.org/10.1021/acs.inorgchem.0c01405.

Tosato, M., Gandini, A., Happel, S., Bas, M., Donzella, A., Zenoni, A., Salvini, A., Andrighetto, A., Di Marco, V., Asti, M., 2023. Chromatographic separation of silver-111 from neutron-irradiated palladium target: toward direct labeling of radiotracers. EJNMMI Radiopharm. Chem. 8 (1), http://dx.doi.org/10.1186/s41181-023-00232-0.

Tosato, M., Verona, M., Favaretto, C., Pometti, M., Zanoni, G., Scopelliti, F., Cammarata, F.P., Morselli, L., Talip, Z., van der Meulen, N.P., Di Marco, V., Asti, M., 2022. Chelation of theranostic copper radioisotopes with S-Rich macrocycles: From radiolabelling of copper-64 to in vivo investigation. Molecules 27 (13), http://dx.doi.org/10.3390/molecules27134158, URL https://www.mdpi.com/1420-3049/27/13/4158.

Vizard, D.L., Helfer, J.N., McLaughlin, W.E., Steklenski, D.J., 1998. Electronic imaging system for autoradiography. URL https://patents.google.com/patent/US6346707B1/en.

Xue, Y., Gao, Y., Meng, F., Luo, L., 2021. Recent progress of nanotechnology-based theranostic systems in cancer treatments. Cancer Biol. Med. 18 (2), 336–351. http://dx.doi.org/10.20892/j.issn.2095-3941.2020.0510, arXiv:https://www.cancerbiomed.org/content/18/2/336.full.pdf. URL https://www.cancerbiomed.org/content/18/2/336.